

# Weak gravitational lensing in the standard Cold Dark Matter model, using an algorithm for three-dimensional shear

Andrew J. Barber<sup>1\*</sup>, Peter A. Thomas<sup>1</sup> and H. M. P. Couchman<sup>2</sup>

<sup>1</sup>*Astronomy Centre, University of Sussex, Falmer, Brighton, BN1 9QJ*

<sup>2</sup>*Dept. of Physics & Astronomy, Univ. of Western Ontario, London, Ontario, N6A 3K7, Canada*

Accepted 1998 —. Received 1998 —; in original form 1998 —

## ABSTRACT

We investigate the effects of weak gravitational lensing in the standard Cold Dark Matter cosmology, using an algorithm which evaluates the shear in three dimensions. The algorithm has the advantage of variable softening for the particles, and our method allows the appropriate angular diameter distances to be applied to every evaluation location within each three-dimensional simulation box. We investigate the importance of shear in the distance-redshift relation, and find it to be very small. We also establish clearly defined values for the smoothness parameter in the relation, finding its value to be at least 0.88 at all redshifts in our simulations. From our results, obtained by linking the simulation boxes back to source redshifts of 4, we are able to observe the formation of structure in terms of the computed shear, and also note that the major contributions to the shear come from a very broad range of redshifts. We show the probability distributions for the magnification, source ellipticity and convergence, and also describe the relationships amongst these quantities for a range of source redshifts. We find a broad range of magnifications and ellipticities; for sources at a redshift of 4, 97½% of all lines of sight show magnifications up to 1.3 and ellipticities up to 0.195. There is clear evidence that the magnification is not linear in the convergence, as might be expected for weak lensing, but contains contributions from higher order terms in both the convergence and the shear.

**Key words:** Galaxies: clustering — Cosmology: miscellaneous — Cosmology: gravitational lensing — Methods: numerical — Large-scale structure of Universe

## 1 INTRODUCTION

The gravitational lensing of light by the general form of the large-scale structure in the universe is of considerable importance in cosmology. This ‘weak lensing’ may result in magnification of a distant source from Ricci focusing due to matter in the beam, and shear leading to distortion of the image cross-section. The strength of these effects depends on the lens and source angular diameter distances and the specific distribution of matter between the observer and source. Consequently the effects are likely to be sensitive to the particular cosmological model. In extreme cases, a source may be strongly lensed if the light passes close to a massive structure such as a galaxy, and this occasionally results in the appearance of multiple images of the source. One of the most important applications of such ‘strong lensing’ studies has

been the reconstruction of mass profiles for lensing galaxies and estimations of the Hubble parameter,  $H_0$ , from measurements of the time-delay between fluctuations in the multiple images of a background quasar; see, e.g., Falco, Govenstein and Shapiro (1991), Grogan and Narayan (1996), and Keeton and Kochanek (1997). These studies have frequently made use of the ‘thin-screen approximation’ in which the depth of the lens is considered to be small compared with the distances between the observer and the lens and the lens and the source. In the thin-screen approximation the mass distribution of the lens is projected along the line of sight and replaced by a mass sheet with the appropriate surface density profile. Deflections of the light from the source are then considered to take place only within the plane of the mass sheet, making computations for the light deflections much simpler.

The simplicity of the thin-screen approximation has also lead to its use in weak gravitational lensing studies, where

\* Email: abarber@star.cpes.susx.ac.uk

the output volumes from cosmological  $N$ -body simulations are treated as planar projections of the particle distributions within them. However, the procedures have to be extended when dealing with the propagation of light from very distant sources, where a number of simulation time outputs are necessary to cover the observer-source distance. In these cases each simulation volume is replaced by a planar projection of the particle distribution, and to compute the distributions in magnification and shear for a large number of rays passing through the system of screens, use is made of the multiple lens-plane theory which has been variously described by Blandford and Narayan (1986), Blandford and Kochanek (1987), Kovner (1987), Schneider and Weiss (1988a, b), and summarised by Schneider, Ehlers and Falco (1992). We describe some of these two-dimensional weak lensing methods in Section 1.1.

Couchman, Barber and Thomas (1998) considered some of the shortcomings of these two-dimensional lens-plane methods, and also rigorously investigated the conditions under which two-dimensional methods would give equivalent results to integrating the shear components<sup>†</sup> through the depth of a simulation volume. They showed that, in general, it is necessary to include the effects of matter stretching well beyond a single period in extent, orthogonal to the line of sight, but depending on the particular distribution of matter. It is also necessary to project the matter contained within a full period onto the plane, assuming the distribution of matter in the universe to be periodic with periodicity equal to the simulation volume side dimension. They also showed that errors can occur in two-dimensional approaches because of the single angular diameter distance to each plane, rather than specific angular diameter distances to every location in the simulation volume.

These considerations motivated Couchman et al. (1998) to develop an algorithm to evaluate the shear components at a large number of locations within the volume of cubic particle simulation time-slices. The algorithm they developed is based on the standard P<sup>3</sup>M method (as described in Hockney and Eastwood, 1988), and uses a Fast Fourier Transform (FFT) method for speed. It is designed to compute the six independent three-dimensional shear components, and therefore represents a significant improvement over two-dimensional methods. We describe the three-dimensional shear algorithm in outline in Section 2.1.

In this paper we have applied the algorithm to the standard Cold Dark Matter (sCDM) cosmological  $N$ -body simulations available from the Hydra consortium,<sup>‡</sup> which we describe in Section 2.2. By combining the outputs from the algorithm from sets of linked time-slices going back to a redshift of 4, we are able to evaluate the overall shear, convergence, magnifications and source ellipticities (and distributions for these quantities). We first describe other work which has generated results from studies of weak lensing in the sCDM cosmology.

<sup>†</sup> Note that, throughout this paper we refer to the elements of the matrix of second derivatives of the gravitational potential as the ‘shear’ components, although, strictly, the term ‘shear’ refers to combinations of these elements which give rise to anisotropy.

<sup>‡</sup> <http://coho.astro.uwo.ca/pub/data.html>

## 1.1 Other work

There are numerous methods for studying weak gravitational lensing. In ‘ray-tracing,’ (see, for example, Schneider and Weiss, 1988b, Jaroszyński et al., 1990, Wambsganss, Cen and Ostriker, 1998, and Marri and Ferrara, 1998, the paths of individual light rays are traced backwards from the observer as they are deflected at each of the projected time-slice planes. The mapping of these rays in the source plane then immediately gives information about the individual amplifications which apply. In the ‘ray-bundle’ method, (see, for example, Fluke, Webster and Mortlock, 1998a, b, and Premadi, Martel and Matzner, 1998a, b, c), bundles of rays representing a circular image are considered together, so that the area and shape of the bundle at the source plane, (after deflections at the intermediate time-slice planes), gives the required information on the ellipticity and magnification. There are also many different procedures for computing the deflections and shear, although most apply the multiple lens-plane theory to obtain the overall magnifications and distributions. We shall describe briefly four works which have produced weak lensing results in the sCDM cosmology.

Jaroszyński et al. (1990) use the ray-tracing method with two-dimensional planar projections of the time-slices, and by making use of the assumed periodicity in the particle distribution, they translate the planes for each ray, so that it becomes centralised in the plane. This ensures that there is no bias acting on the ray when the shear is computed. Each plane is divided into a regular array of pixels, and the column density in each pixel is evaluated. Instead of calculating the effect of every particle on the rays, the pixel column densities in the single period plane are used. They calculate the two two-dimensional components of the shear (see Section 5 for the definition of shear) as ratios of the mean convergence of the beam, which they obtain from the mean column density. However, they have not employed the net zero mean density requirement in the planes, (described in detail by Couchman et al., 1998), which ensures that deflections and shear can only occur when there are departures from homogeneity. Also, the matter in the pixel through which the ray is located is excluded. Their probability distributions for the convergence, due to sources at redshifts of 1, 3 and 5, are therefore not centralised around zero, and exhibit only limited broadening for sources at higher redshift. They also display the probability distributions for the shear and the corresponding distributions for source ellipticity. The procedures used by Jaroszyński (1991) and Jaroszyński (1992) are improved by the introduction of softening to each particle to represent galaxies of different masses and radii with realistic correlations in position. In these papers Monte Carlo methods are used to study the effects of weak lensing on the propagation of light through inhomogeneous particle distributions.

Wambsganss et al. (1998) also use the ray-tracing method with two-dimensional planar projections of the simulation boxes, which have been randomly oriented. Rays are shot through the central region of  $8h^{-1}\text{Mpc} \times 8h^{-1}\text{Mpc}$  only, (where  $h$  is the Hubble parameter expressed in units of  $100 \text{ km s}^{-1} \text{ Mpc}^{-1}$ ), and the deflections are computed by including all the matter in each plane, allocated to pixels  $10h^{-1}\text{kpc} \times 10h^{-1}\text{kpc}$ , covering one period in extent only. The planes have comoving dimensions of  $80h^{-1}\text{Mpc} \times 80h^{-1}\text{Mpc}$ . The

computations make use of a hierarchical tree code to collect together those matter pixels far away, whilst the nearby ones are treated individually, and the code assumes that all the matter in a pixel is located at its centre of mass. By using the multiple lens-plane theory, they show both the differential magnification probability distribution, and the integrated one for 100 different source positions at redshift  $z_s = 3.0$ . One advantage of this type of ray-tracing procedure is its ability to indicate the possibility of multiple imaging, where different rays in the image plane can be traced back to the same pixel in the source plane.

Premadi, Martel and Matzner (1998a) have improved the resolution of their  $N$ -body simulations by using a Monte Carlo method to locate individual galaxies inside the computational volume, and ensuring that they match the 2-point correlation function for galaxies. They also assign morphological types to the galaxies according to the individual environment, and apply a particular surface density profile for each. To avoid large scale structure correlations between the simulation boxes, five different sets of initial conditions are used for the simulations, so that the individual plane projections can be selected at random from any set. By solving the two-dimensional Poisson equation on a grid, and inverting the equation using a FFT method, they obtain the first and second derivatives of the gravitational potential on each plane. They also correctly ensure that the mean surface density in each lens-plane vanishes, so that a good interpretation of the effects of the background matter is made. Their method uses beams of light, each comprising 65 rays arranged in two concentric rings of 32 rays each, plus a central ray. To obtain good statistical data they have run their experiment for 500 beams. They show the average shear for a source at  $z_s = 5$  contributed by each of the lens-planes individually, and find that the largest contributions come from those planes at intermediate redshift, of order  $z=1-2$ . Similarly, they find that the lens-planes which contribute most to the average magnifications are also located at intermediate redshifts. The multiple lens-plane theory then enables the distributions of cumulative magnifications to be obtained, which are shown to be broad and similar in shape for the  $s$ CDM and cosmological constant models, although the latter model shows a shift to larger magnification values.

Marri and Ferrara (1998) use a total of 50 lens-planes evenly spaced in redshift up to  $z = 10$ . Their mass distributions have been determined by the Press-Schechter formalism (which they outline), which is a complementary approach to  $N$ -body numerical simulations. From this method they derive the normalised fraction of collapsed objects per unit mass for each redshift. They acknowledge that the Press-Schechter formalism is unable to describe fully the complexity of extended structures, the density profile of the collapsed objects (the lenses), or their spatial distribution at each redshift. They therefore make the assumption that the lenses are spatially uncorrelated and randomly distributed on the planes, and furthermore behave as point-like masses with no softening. The maximum number of lenses in a single plane is approximately 600, each having the appropriate computed mass value. In their ray-tracing approach they follow  $1.85 \times 10^7$  rays uniformly distributed within a solid angle of  $2.8 \times 10^{-6}$  sr, corresponding to a  $420'' \times 420''$  field. The final impact parameters of the rays are collected in an orthogonal grid of  $300^2$  pixels in the source plane. Because

of the use of point masses, their method produces very high magnification values, greater than 30 for the  $s$ CDM cosmology. They have also chosen to use a smoothness parameter  $\bar{\alpha} = 0$  in the redshift-angular diameter distance relation (which we describe in Section 3) which depicts an entirely clumpy universe.

## 1.2 Outline of paper

In Section 2.1 we summarise the main features of the algorithm for shear in three dimensions, which is detailed in Couchman et al. (1998). Because the code is applied to evaluation positions within the volume of  $N$ -body simulation boxes, we are able to apply specific appropriate angular diameter distances to each location, which is not possible with two-dimensional planar projections of simulation boxes. We also note that the algorithm automatically includes the effects of the periodic images of the fundamental simulation volume, so that the results for the shear are computed for matter effectively stretching to infinity. Included also is the net zero mean density requirement, which ensures that deflections and shear may only occur as a result of departures from homogeneity. In Section 2.2 we describe the  $s$ CDM  $N$ -body simulations and how we combine the different output time-slices from the simulations to enable the integrated shear along lines of sight to be evaluated. Section 2.3 describes the variable softening facility employed in the code, and our choice of a minimum softening value, which may be given a realistic physical interpretation.

Because we evaluate the shear at locations throughout the volume of the simulation boxes, and because of some sensitivity (see Couchman et al., 1998) of the results to the smoothness, or clumpiness, of the matter distribution in the universe, we consider, in Section 3, our choice of the appropriate angular diameter distances. We consider the effects of shear on the angular diameter distance, and the sensitivity of our results to the smoothness parameter,  $\bar{\alpha}$ . Measurements of the particle clustering within our simulations, which determines the variable softening parameter for use in the shear algorithm, also enable a good definition for the smoothness parameter to be made, and this is discussed.

In Section 4, we describe the formation of structure within the universe as it evolves, in terms of the magnitudes of the shear components computed for each time-slice. We see how the rms values of the components vary with redshift, and also how the set of highest values behave. We also identify, in terms of the lens redshifts, where the significant contributions arise. Our conclusions are compared with the results of other authors.

In Section 5, we describe in outline the multiple lens-plane theory, with particular reference to our application of it. In Section 6, we discuss our results for the shear, convergence, magnifications, source ellipticities, distributions of these values, and relationships amongst them. Section 7 summarises our findings, compares our results with those of other authors for the  $s$ CDM cosmology, and proposes applications of our method and results.

## 2 THE ALGORITHM FOR THREE-DIMENSIONAL SHEAR, AND THE COSMOLOGICAL SIMULATIONS

### 2.1 Description of the three-dimensional algorithm

The algorithm we are using to compute the elements of the matrix of second derivatives of the gravitational potential has been described fully in Couchman et al. (1998). The algorithm is based on the standard P<sup>3</sup>M method, and uses a FFT convolution method. It computes all of the six independent shear component values at each of a large number of selected evaluation positions within a three-dimensional  $N$ -body particle simulation box. The P<sup>3</sup>M algorithm has a computational cost of order  $N \log_2 N$ , where  $N$  is the number of particles in the simulation volume, rather than  $O(N^2)$  for simplistic calculations based on the forces on  $N$  particles from each of their neighbours. For ensembles of particles, used in typical  $N$ -body simulations, the rms errors in the computed shear component values are typically  $\sim 0.3\%$ .

In addition to the speed and accuracy of the shear algorithm, it has the following features.

First, the algorithm uses variable softening designed to distribute the mass of each particle within a radial profile which depends on its specific environment. In this way we are able to set individual mass profiles for the particles which enables a physical depiction of the large scale structure to be made. We describe our choice of the appropriate variable softening in Section 2.3.

Second, the shear algorithm works within three-dimensional simulation volumes, rather than on planar projections of the particle distributions, so that angular diameter distances to every evaluation position can be applied. It has been shown (Couchman et al., 1998) that in specific circumstances, the results of two-dimensional planar approaches are equivalent to three-dimensional values integrated throughout the depth of a simulation box, provided the angular diameter distance is assumed constant throughout the depth. However, by ignoring the variation in the angular diameter distances throughout the box, errors up to a maximum of 9% can be reached at a redshift of  $z = 0.5$  for sCDM simulation cubes of comoving side  $100h^{-1}$  Mpc. (Errors can be larger than this at high and low redshift, but the angular diameter distance multiplying factor for the shear values is greatest here for sources we have chosen at a redshift of 4.)

Third, the shear algorithm automatically includes the contributions of the periodic images of the fundamental volume, essentially creating a realisation extending to infinity. Couchman et al. (1998) showed that it is necessary to include the effects of matter well beyond the fundamental volume in general (but depending on the particular particle distribution), to achieve accurate values for the shear. Methods which make use of only the matter within the fundamental volume may suffer from inadequate convergence to the limiting values.

Fourth, the method uses the ‘peculiar’ gravitational potential,  $\phi$ , through the subtraction of a term depending upon the mean density. Such an approach is equivalent to requiring that the net total mass in the system be set to zero, and ensures that we deal only with light ray deflections arising

from departures from homogeneity; in a pure Robertson-Walker metric we would want no deflections.

### 2.2 The sCDM large scale structure simulations

We have chosen, in this paper, to apply the shear algorithm to the sCDM cosmological  $N$ -body simulations available from the Hydra consortium, and produced using the ‘Hydra’  $N$ -body hydrodynamics code, as described by Couchman, Thomas and Pearce (1995). Each time-slice from this simulation contains  $128^3$  dark matter particles, each of  $1.2 \times 10^{11} h^{-1}$  solar masses, with a CDM spectrum in an Einstein-de Sitter universe, and has comoving box sides of  $100h^{-1}$  Mpc. The output times for each time-slice have been chosen so that consecutive time-slices abut, enabling a continuous representation of the evolution of large scale structure in the universe. However, to avoid unrealistic correlations of the structure through consecutive boxes, we arbitrarily rotate, reflect and translate the particle coordinates in each before the boxes are linked together. We have chosen to analyse all the simulation boxes back to a redshift of 3.9, a distance which is covered by a continuous set of 33 boxes (assuming the source in this case at  $z_s = 3.9$  to be located at the far face of the 33rd box, which has a nominal redshift of 3.6). The simulations used have a power spectrum shape parameter of 0.25 as determined experimentally on cluster scales, (see Peacock and Dodds, 1994), and the normalisation,  $\sigma_8$ , has been taken as 0.64 to reproduce the number density of clusters, according to Vianna and Liddle (1996).

We establish a regular array of  $100 \times 100$  lines of sight through each simulation box, and compute the six independent shear components at 1000 evenly spaced evaluation positions along each. Since we are dealing with weak lensing effects and are interested only in the statistical distribution of values, these lines of sight adequately represent the trajectories of light rays through each simulation box. It is sufficient also to connect each ‘ray’ with the corresponding line of sight through subsequent boxes in order to obtain the required statistics of weak lensing. This is justified because of the random re-orientation of each box performed before the shear algorithm is applied.

### 2.3 Variable softening

The variable softening facility in the code allows each particle to be treated individually as an extended mass, and the softening parameter applied to each is chosen to be proportional to the distance,  $l$ , to the particle’s 32nd nearest neighbour. In this way the softening is representative of the density environment of each particle. The appropriate value of the parameter is determined using a different smoothed particle hydrodynamics (SPH) programme. The shear algorithm then works with the ratio of the chosen softening for each particle to the maximum value (equivalent to the mesh dimension, which is defined by the regular grid laid down to decompose the short- and long-range force calculations), so that the parameter has a maximum value of unity in the code.

Isolated particles are therefore assigned large softening values, and are then not able to cause anomalous strong deflections. In addition, this helps to ensure that more rays

pass through regions of softened mass rather than voids of negative density. Particles in denser regions are assigned correspondingly smaller softening scales, and are therefore able to cause stronger deflections. In the regions of highest density we choose to set a minimum value for the softening, to avoid interpolation errors in the code for very small separations, and to introduce a physically realistic scale size to such particles.

In the  $s$ CDM simulation we have used, the minimum values for  $l$  are of order  $10^{-3}$  in box units, and for a large cluster of 1000 particles this is comparable to the maximum value of the Einstein radius for lenses up to a redshift of 4. (For our maximum source redshift of 3.9, and for a lens of 1000 particles in our simulation, the Einstein radius reaches a maximum of  $0.11h^{-1}$  Mpc, or 0.0011 box units, at a redshift of 0.52.) Hence, by choosing a minimum for the variable softening of this order, we would rarely expect to see strong lensing. At the same time, this scale is approximately of galactic dimensions, thereby giving a realistic interpretation to the choice.

We have therefore set the minimum level to 0.001 in box units, and allowed it to remain at a fixed physical dimension throughout the redshift range of the simulations. Thus, we have set the value to be 0.001 for the  $z = 0$  simulation box, rising to 0.0046 in the earliest simulation box at  $z = 3.6$ .

Couchman et al. (1998) describes also the sensitivity of the magnification distributions to the choice of minimum softening arising from a single, assumed isolated, simulation box, and shows that the results are insensitive to minimum softenings of 0.001 and 0.002, apart from the peak magnification values, which occur only in limited numbers of lines of sight. This is very useful because we can assume that our results are likely to be little different from those using the same minimum softening throughout, whilst keeping the value fixed in physical size gives a credible interpretation to the softening.

### 3 ANGULAR DIAMETER DISTANCES

One of the advantages of being able to evaluate the shear components at a large number of locations within the volume of each time-slice is that we are able to apply the appropriate angular diameter distance factors to each as part of the procedure to determine the magnifications and ellipticities. The elements of the Jacobian matrix, at each evaluation position,

$$\mathcal{A} = \begin{pmatrix} 1 - \psi_{11} & -\psi_{12} \\ -\psi_{21} & 1 - \psi_{22} \end{pmatrix}, \quad (1)$$

(from which the magnification may be derived at any point), contains the two-dimensional effective lensing potentials which are related to the computed three-dimensional shear through

$$\psi_{ij} = \frac{D_d D_{ds}}{D_s} \cdot \frac{2}{c^2} \int \frac{\partial^2 \phi(z)}{\partial x_i \partial x_j} dz, \quad (2)$$

where  $D_d$ ,  $D_{ds}$ , and  $D_s$  are the angular diameter distances from the observer to the lens, the lens to the source, and the observer to the source, respectively, and  $c$  is the velocity of light. (The factor  $D_d D_{ds} / D_s$  may be written equivalently as  $cR/H_0$ , where  $R$  is dimensionless.) The integration is along

the line of sight. The angular diameter distance of the source is defined to be the distance inferred from its angular size, assuming Euclidean geometry, and in an expanding universe this distance becomes a function of the redshift of the source. The angular diameter distance also depends very much on the distribution of matter; for example, excess matter within the beam causes it to become more focussed, making the source appear closer than it really is. It is therefore necessary to have available appropriate values for the angular diameter distances for the particular distribution of matter in the simulation data-set being investigated.

Schneider et al. (1992) summarise clearly the work of Dyer and Roeder (1972, 1973) who made assumptions about the type of matter distribution to obtain a second order differential equation for the angular diameter distance in terms of the density parameter,  $\Omega$ , for the universe, and the redshift of the source:

$$(z+1)(\Omega z+1) \frac{d^2 D}{dz^2} + \left( \frac{7}{2} \Omega z + \frac{\Omega}{2} + 3 \right) \frac{dD}{dz} + \left( \frac{3}{2} \bar{\alpha} \Omega + \frac{|\sigma|^2}{(1+z)^5} \right) D = 0. \quad (3)$$

$\bar{\alpha}$  is the smoothness parameter, which is taken to be the fraction of mass in the universe which is smoothly distributed, so that a fraction  $(1 - \bar{\alpha})$  is considered to be bound into clumps.  $\sigma$  is the optical scalar for the shear, introduced by matter surrounding the beam.

Dyer and Roeder considered the convenient scenario in which the light beams travel through the homogeneous low density, or empty regions, passing far away from the clumps, so that the shear becomes negligible. However, we must consider whether the shear in our particle simulation time-slices is able to significantly affect our chosen values for the angular diameter distances.

Schneider and Weiss (1988a) performed Monte Carlo simulations to determine the amplification of sources in a clumpy universe made up of several lens-planes, each containing a random distribution of point-like particles. They were able to show that the fraction of ‘empty cones,’ i.e., possible ray trajectories far from the clumps with negligible shear, in a clumpy universe is small, so that in general, the effects of shear must be taken into account in the expression for the angular diameter distances. For rays weakly affected by shear and with low amplifications, the linear terms in the shear almost cancel, but higher order terms become more important. However, the probability for rays being affected by shear is dramatically lower in model universes with  $\bar{\alpha} = 0.8$  compared with universes with  $\bar{\alpha} = 0$ . (We shall show shortly that the values of  $\bar{\alpha}$  in our  $s$ CDM simulations are always at least 0.88, so that even at  $z = 0$  the matter distribution may be considered smooth according to the usual definition of  $\bar{\alpha}$ .) In summary, we might expect the number of rays affected by shear to be low in smooth matter distributions, and then the effect to be only of second order. Schneider and Weiss (1988a) also derive an integral equation for the angular diameter distance which they show to be equivalent to that of Dyer and Roeder (1973) (without the shear term) when measured through the ‘empty cones.’

Watanabe and Tomita (1990) numerically solve the null geodesic equations for light passing through a spatially flat Einstein-de Sitter background universe in which the matter is condensed into (softened) compact objects of galactic or

galactic cluster dimensions, and having an average specified separation in the present epoch. Their conclusion, that, on average, the effect of shear on the distance-redshift relation is small, providing the scale of the inhomogeneities is greater than or equal to galactic scales, agrees also with those of Futamase and Sasaki (1989), who show that, in most cases, the shear does not contribute to the amplification. This conclusion remains valid even when the density contrast is greater than unity, although in the model used by Watanabe and Tomita (1990) all amplifications were less than 2.

Our own work is conducted using a cosmological simulation in which the distribution of matter is very smooth. Furthermore, our minimum softening scale is of the order of galactic dimensions, so that we feel justified in accepting that the shear plays only a second order role in the distance-redshift relation in our  $\Lambda$ CDM data-set. (We are able to quantify the effects of shear from our results in Section 6, and find that they are negligible.) With  $\sigma \sim 0$ , therefore, equation (3) immediately reduces to the well-known Dyer-Roeder equation. However, we also need to establish a value for the smoothness parameter in our simulations, so that the appropriate angular diameter distances can be evaluated and applied to the data. Assuming  $\sigma = 0$ , Schneider et al. (1992) give the following generalised solution of the Dyer-Roeder equation for the angular diameter distance between redshifts of  $z_1$  and  $z_2$  for  $\Omega = 1$ :

$$D(z_1, z_2) = \frac{c}{H_0} \frac{1}{2\beta} \left[ \frac{(1+z_2)^{\beta-\frac{5}{4}}}{(1+z_1)^{\beta+\frac{1}{4}}} - \frac{(1+z_1)^{\beta-\frac{1}{4}}}{(1+z_2)^{\beta+\frac{5}{4}}} \right], \quad (4)$$

in which  $\beta$  is expressed in terms of arbitrary  $\bar{\alpha}$ :

$$\beta = \frac{1}{4}(25 - 24\bar{\alpha})^{\frac{1}{2}}. \quad (5)$$

We can write the left hand side of equation 4, equivalently, as  $D(z_1, z_2) = \frac{c}{H_0} r(z_1, z_2)$ , in which  $r(z_1, z_2)$  is the dimensionless angular diameter distance. We show in Figure 1 the value of the dimensionless multiplying factor,  $R = r_d r_{ds} / r_s$ , as it applies to different time-slices at different redshifts, assuming sources at  $z_s = 3.9, 3.0, 1.9, 1.0$  and  $0.5$ . (These values correspond to the redshifts of our time-slices, and have been chosen to be close to  $z = 4, 3, 2, 1$  and  $0.5$ .) We have assumed zero shear, a completely smooth distribution of matter, ( $\bar{\alpha} = 1$ ), and  $\Omega = 1$ . We see that the peak in this factor occurs near  $z = 0.5$  for a source at redshift 4.

From the output of our algorithm we are able to obtain an estimate of the clumpiness or smoothness in each time-slice. Having set the minimum softening scale, the code declares the number of particles which are assigned the minimum softening, and we can therefore immediately obtain the mass fraction contained in clumps, which we choose to define by the minimum softening scale.

In the earliest time-slice at  $z = 3.6$ , (next to  $z = 3.9$ ), there is a mass fraction of only  $5.6 \times 10^{-3}$  in clumps, giving  $\bar{\alpha}(z = 3.6) = 0.99$ , and at  $z = 0$  the fraction is 0.12, giving  $\bar{\alpha}(z = 0) = 0.88$ . Whilst we have not accurately tried to assess the mean value for  $\bar{\alpha}$  extending to different source redshifts, it is clear that the value throughout is very close to 1, and almost equivalent to the ‘filled beam’ approximation. This result concurs with Tomita (1998) who solves the null-geodesic equations for a large number of pairs of light rays in four different cosmological simulations with the  $\Lambda$ CDM spectrum. He uses  $32^3$  particles in each, softened to various

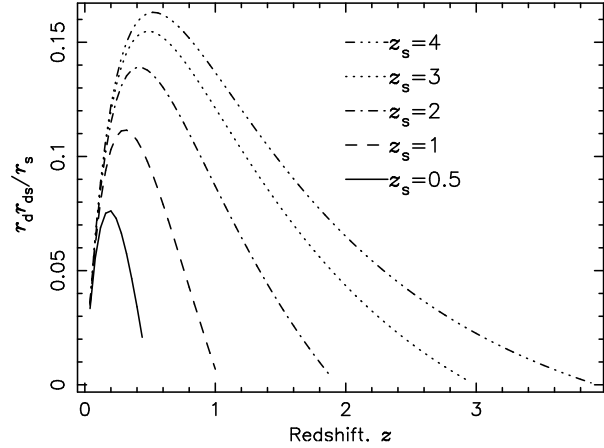


**Figure 1.** The dimensionless multiplying factor,  $R = r_d r_{ds} / r_s$ , assuming sources at different redshifts. The uppermost curve for a source at  $z_s = 4$ , peaks at  $z = 0.52$ ; the next curve is for  $z_s = 3$  and peaks at  $z = 0.48$ ; the next curve is for  $z_s = 2$  and peaks at  $z = 0.40$ ; the next curve is for  $z_s = 1$  and peaks at  $z = 0.32$ ; the lowest curve is for  $z_s = 0.5$  and peaks at  $z = 0.20$ .

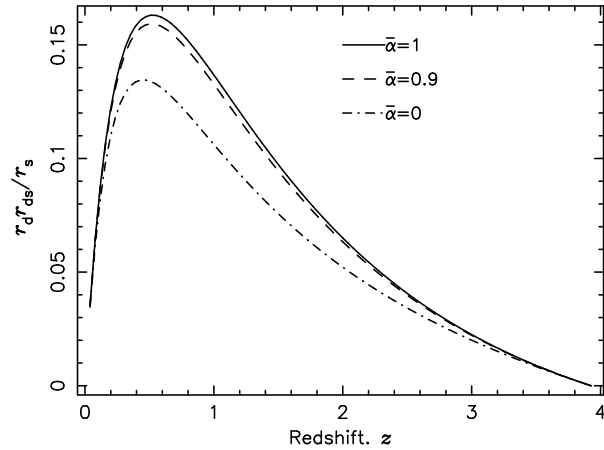


**Figure 2.** The multiplying factor,  $r_d r_{ds} / r_s$ , for a source at redshift 4, with smoothness parameters of 1 (uppermost curve), 0.9 (middle curve), and 0 (lowest curve).

physical radii up to a maximum of  $40h^{-1}$  kpc, and finds  $\bar{\alpha}$  to be close to 1 in all cases. However, there does appear to be considerable dispersion in the values at late times. We show in Figure 2 how similar the multiplying factor is for the values  $\bar{\alpha} = 0.9$  and  $1.0$ , and how these compare with a value of  $\bar{\alpha} = 0$  for an entirely clumpy universe. The discrepancy at the peak between  $\bar{\alpha} = 0.9$  and  $\bar{\alpha} = 1.0$  is 3.1%.

Figure 3 shows the ratio of the multiplying factor for  $\bar{\alpha} = 1$  and  $\bar{\alpha} = 0.9$  for the various source redshifts. For sources at  $z_s = 2$  the maximum value of the ratio is 1.014, and for sources nearer than  $z_s = 1$  the discrepancy is well below 1%.

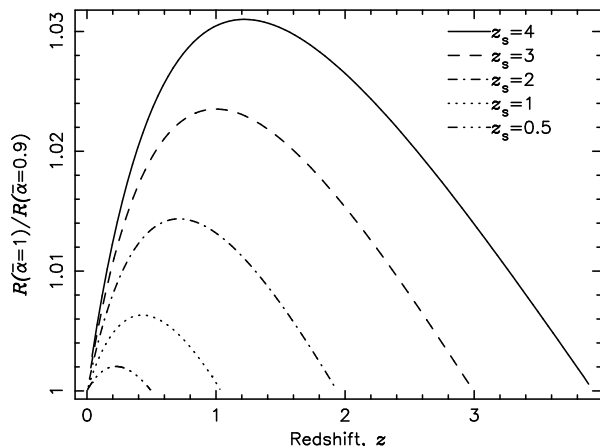


**Figure 3.** The ratio of the dimensionless angular diameter distance multiplying factors,  $R$ , with  $\bar{\alpha} = 1$  and  $\bar{\alpha} = 0.9$ , for sources at redshifts 4, 3, 2, 1, and 0.5. The values of the ratio at the peaks of these curves are 1.031, 1.024, 1.014, 1.006 and 1.002 respectively.

#### 4 THE FORMATION OF STRUCTURE

The shear algorithm generates the six independent three-dimensional shear component values (expressed in box units), and we have chosen to compute them at 1000 evaluation positions along  $100 \times 100$  lines of sight in each simulation time-slice. In a simplistic way, the magnitude of these components characterises the particular time-slice. To convert the components to absolute values we have to apply the appropriate angular diameter distance factors,  $R = r_d r_{ds} / r_s$ , as described in the previous section, together with the factor  $B(1+z)^2$ , where  $B = 3.733 \times 10^{-9}$  for the simulation boxes we have used (which have comoving dimensions of  $100h^{-1}$  Mpc) and where the  $(1+z)^2$  factor occurs to convert the comoving code units to physical units.

The magnitude of the rms value determined from each component multiplied by  $B(1+z)^2$  in each time-slice is then of interest. In Figure 4 we show these values for the sum of the diagonal terms in the (projected) matrix of effective lensing potentials; this is closely associated with the surface density, which in turn determines the magnifications produced in the time-slice. We notice that the values for these combined components very slowly decreases towards  $z = 0$ . This same trend is apparent with the other components individually. It has the interesting interpretation that, even though structure is forming (to produce greater magnification locally), the real expansion of the universe (causing the mean particle separation to increase) just outweighs this in terms of the magnitudes of the component values. Nevertheless, the formation of structure can be seen; by considering just the sets of highest values in each time-slice, again multiplied by the factor  $B(1+z)^2$ , and taking the mean values of these, we see in Figure 4 an initial fall as the universe expands and before structure has begun to form, and then at later times an increase in the mean values, indicative of the existence of dense (bound) structures.

However, when the values are then multiplied by the angular diameter distance factor,  $R$ , we see in Figure 5 that

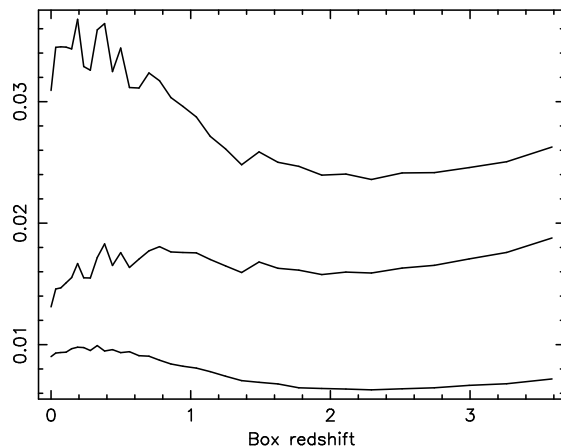


**Figure 4.** Middle curve: the rms value in each time-slice, multiplied by  $B(1+z)^2$ , of the sum of the diagonal components of the two-dimensional shear components, showing a gradual fall towards  $z = 0$ . Top curve: The set of highest values of the summed diagonal components, multiplied by  $B(1+z)^2$ , which shows the initial gradual fall as the universe expands, and then an increase towards  $z = 0$  as structure forms. Lowest curve: The set of highest values for one of the off-diagonal components, multiplied by  $B(1+z)^2$ , which shows a similar trend to the top curve.

the peaks are extremely broad, indicating that significant contributions to the magnifications and ellipticities can arise in time-slices covering a wide range of redshifts, and not just near  $z = 0.5$  where  $R$  has its peak (for sources at  $z_s = 4$ ).

Premadi, Martel and Matzner (1998a) have done similar work, using 5 different sets of initial conditions for each of their  $N$ -body simulations, so that the time-slices can be chosen at random from any one of the 5 sets, randomly translated to avoid correlations in the large scale structure between adjacent boxes, and projected onto planes. They solve the two-dimensional Poisson equation on a grid, and use a FFT method to obtain the first and second derivatives of the gravitational potential on each plane. They consider the effects on light beams, each consisting of 65 rays arranged in concentric rings to represent circular images, and have performed 500 calculations for each cosmological model, based on 500 different random translations of the planes. For the shear and magnification they find that the individual contribution due to each lens-plane is greatest at intermediate redshifts, of order  $z = 1 - 2$ , for sources located at  $z_s = 5$ .

Premadi, Martel and Matzner (1998b, c) also report their results for the shear for sources at  $z_s = 3$ , and again find very broad peaks covering a wide range of (intermediate) lens-plane redshifts.

#### 5 MULTIPLE LENS-PLANE THEORY

As described in Section 2.2, we establish 1000 evaluation positions along each of the  $100 \times 100$  lines of sight through each simulation time-slice, and the shear algorithm computes the six independent second derivatives of the gravitational potential at each position. By integration of the values we establish the matrix of two-dimensional effective lensing

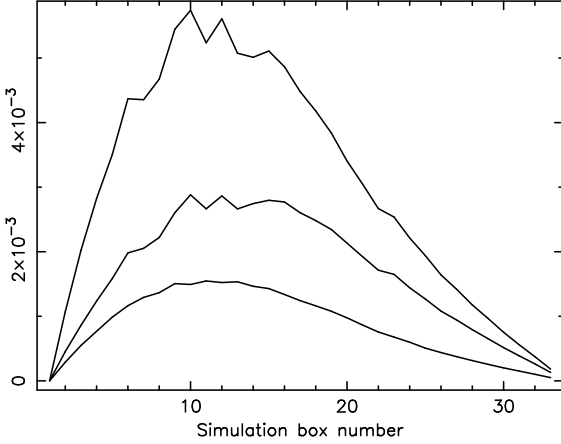


**Figure 5.** Components in each time-slice converted to absolute values, including the angular diameter distance factors, for sources at  $z_s = 4$ . Middle curve: the rms value for each time-slice of the sum of the diagonal components of the two-dimensional shear components. Top curve: The set of highest values of the summed diagonal components. Lowest curve: The set of highest values for one of the off-diagonal components. All the curves are seen to exhibit extremely broad peaks, indicative of significant contributions from a wide range of redshifts. (Box 10 is at redshift 0.3835, and box 20 is at redshift 1.1400.)

potentials at each of 50 positions along every line of sight. We establish the Jacobian matrix,  $\mathcal{A}$ , from these effective lensing potentials by applying the appropriate multiplying factors, as described in Section 3, and the Jacobian develops along the line of sight for each evaluation position. It is computed recursively in accordance with the multiple lens-plane theory, which is summarised by Schneider et al. (1992). The final Jacobian matrix after  $N$  deflections is

$$\mathcal{A}_{\text{total}} = \mathcal{I} - \sum_{i=1}^N \mathcal{U}^i \mathcal{A}_i, \quad (6)$$

where  $\mathcal{I}$  is the unit matrix,

$$\mathcal{U}^i = \begin{pmatrix} \psi_{11}^i & \psi_{12}^i \\ \psi_{21}^i & \psi_{22}^i \end{pmatrix} \quad (7)$$

for the  $i$ th deflection, and the intermediate Jacobian matrices are

$$\mathcal{A}_j = \mathcal{I} - \sum_{i=1}^{j-1} \beta_{ij} \mathcal{U}_i \mathcal{A}_i, \quad (8)$$

where

$$\beta_{ij} = \frac{D_s D_{ij}}{D_{is} D_j}, \quad (9)$$

in which  $D_j$ ,  $D_{is}$  and  $D_{ij}$  are the angular diameter distances to the  $j$ th lens, that between the  $i$ th lens and the source, and that between the  $i$ th and  $j$ th lenses, respectively.

The magnification,  $\mu$ , at any position, is given in terms of the Jacobian at that point:

$$\mu = (\det \mathcal{A})^{-1}, \quad (10)$$

so that we can assess the magnification as it develops along a line of sight, finally computing the emergent magnification

after passage through an entire box or set of boxes. The convergence,  $\kappa$ , is defined by

$$\kappa = \frac{1}{2}(\psi_{11} + \psi_{22}) \quad (11)$$

from the diagonal elements of the Jacobian matrix, and causes isotropic focussing of light rays, and so isotropic magnification of the source. Thus, with convergence acting alone, the image would be the same shape as, but a different size from, the source.

The shear,  $\gamma$ , in each line of sight, is given by

$$\gamma^2 = \gamma_1^2 + \gamma_2^2 \equiv \frac{1}{4}(\psi_{11} - \psi_{22})^2 + \psi_{12}^2. \quad (12)$$

Shear introduces anisotropy, causing the image to be a different shape, in general, from the source.

From equation 10, and these definitions,

$$\mu = (1 - \psi_{11} - \psi_{22} + \psi_{11}\psi_{22} - \psi_{12}^2)^{-1}, \quad (13)$$

so that with weak lensing the magnification reduces to

$$\mu \simeq 1 + 2\kappa + 3\kappa^2 + \gamma^2 + O(\kappa^3, \gamma^3). \quad (14)$$

In the presence of convergence and shear, a circular source becomes elliptical in shape, and the ellipticity,  $\epsilon$ , defined in terms of the ratio of the minor and major axes, becomes

$$\epsilon = 1 - \frac{1 - \kappa - \gamma}{1 - \kappa + \gamma}, \quad (15)$$

which reduces to

$$\epsilon \simeq 2\gamma(1 + \kappa - \gamma) + O(\kappa^3, \gamma^3) \quad (16)$$

in weak lensing.

The multiple lens-plane procedure allows values and distributions of the magnification, ellipticity, convergence and shear to be obtained at  $z = 0$  for light rays traversing the set of linked simulation boxes starting from the chosen source redshift. The ability to apply the appropriate angular diameter distances at every evaluation position avoids the introduction of errors associated with planar methods, and also allows the possibility of choosing source positions within a simulation box if necessary. This may be useful when considering the effects of large-scale structure on real observed sources at specific redshifts, or if the algorithm is to be applied to large simulation volumes.

## 6 RESULTS

We first examine the importance of the smoothness parameter,  $\bar{\alpha}$ , in the distance-redshift relation, to the magnification distribution, by computing the magnifications due to a single (assumed isolated) simulation box at  $z = 0.5$  for a source at  $z_s = 4$ . (At this box redshift the contribution to the magnification is expected to be near the maximum.) The magnification distributions arising for  $\bar{\alpha} = 1$  and  $\bar{\alpha} = 0.9$ , (deduced from our simulations, as explained in Section 3) are virtually indistinguishable. The only significant difference is the maximum value of the magnification in each case, which is only 1.9% higher in the  $\bar{\alpha} = 1$  case. We therefore feel justified in presenting our results based on a smoothness parameter of  $\bar{\alpha} = 1$  throughout.

We have chosen to assume source redshifts,  $z_s$ , close to 4, 3, 2, 1 and 0.5, and shall refer to the sources in these



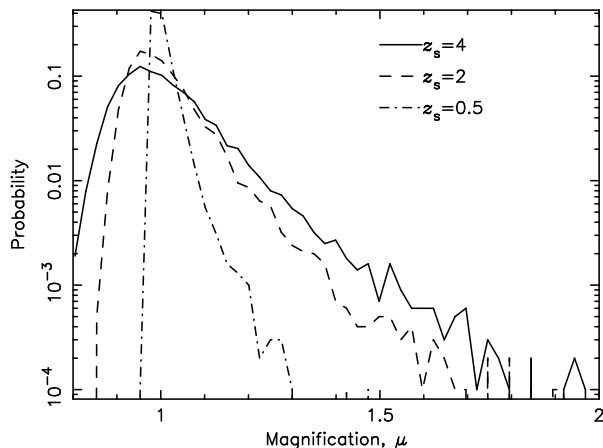


**Figure 6.** Probability distributions for the magnification, for  $z_s = 4, 2$  and  $0.5$ .

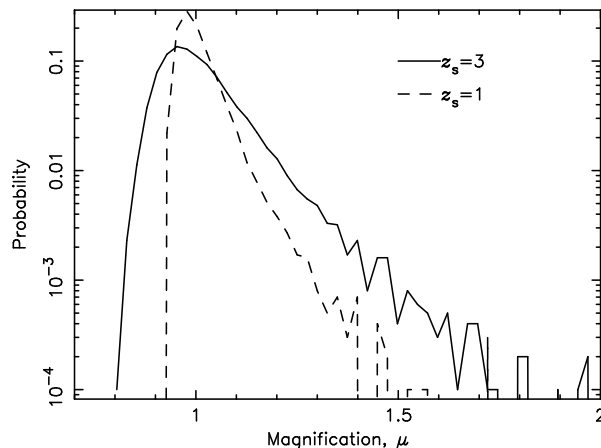


**Figure 7.** Probability distributions for the magnification, for  $z_s = 3, 1$ .

$z_s$	$\mu_{\text{rms}}$	$\mu_{\text{low}}$	$\mu_{\text{high}}$
4	0.126	0.85	1.30
3	0.111	0.86	1.26
2	0.088	0.88	1.20
1	0.056	0.93	1.13
0.5	0.027	0.97	1.05

**Table 1.** Column 2 shows the rms fluctuations for the magnifications,  $\mu_{\text{rms}}$ , about the mean value of  $\langle \mu \rangle = 1$  for the various source redshifts,  $z_s$ ; column 3 shows the magnification value  $\mu_{\text{low}}$  for each redshift above which  $97\frac{1}{2}\%$  of all lines of sight fall; column 4 shows the magnification values  $\mu_{\text{high}}$  for each redshift below which  $97\frac{1}{2}\%$  of all lines of sight fall;

terms. The actual redshift values are 3.9, 3.0, 1.9, 1.0 and 0.5 respectively, corresponding to nominal time-slice redshifts in our  $s$ CDM simulation. For each source redshift we have evaluated the final emergent Jacobian matrix at  $z = 0$  for all 10000 lines of sight, by linking all the simulation boxes between the source redshift and  $z = 0$ , as described in Section 5, and, by manipulation of the data according to the multiple lens-plane equations, we have been able to produce all the required values for the magnifications, ellipticities, shear and convergence.

Figures 6 and 7 show the distributions of the magnifications,  $\mu$ , for the five source redshifts, and for all source redshifts there is a significant range. The rms fluctuations for the magnifications about the mean value of  $\langle \mu \rangle = 1$  are displayed in column 2 of the table for each source redshift. However, since the magnification distributions are asymmetrical, we have calculated the values,  $\mu_{\text{low}}$  and  $\mu_{\text{high}}$ , above and below which  $97\frac{1}{2}\%$  of all lines of sight fall. These are displayed in columns 3 and 4 of the table.

The accumulating number of lines of sight having magnifications greater than the abscissa value is shown in Figure 8 for the five different source redshifts, and clearly shows the distinctions at the high magnification end.

In Figure 9 we show the magnification,  $\mu$ , plotted

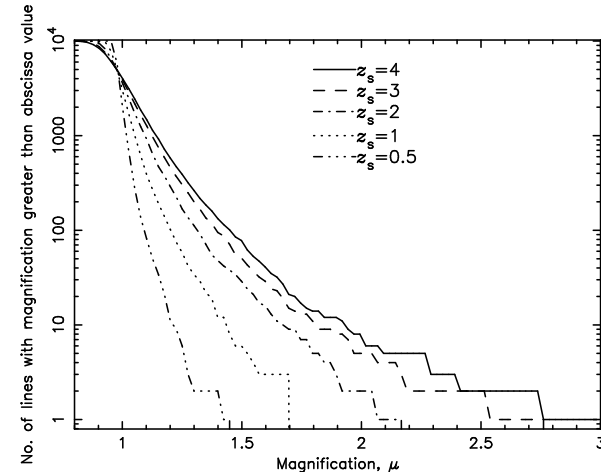


**Figure 8.** The accumulating number of lines of sight with magnifications greater than the abscissa value, for  $z_s = 4, 3, 2, 1$  and  $0.5$ .

against the convergence,  $\kappa$ , for  $z_s = 4$ , and see that the magnification is clearly not linear in  $\kappa$  as expected for small magnitudes of  $\kappa$ . This is true for all our source redshifts except  $z_s = 0.5$ , for which the curve is closely linear throughout. The non-linearity arises because of the presence of the higher order terms in the expression for  $\mu$  given by equation 14, and we show for comparison the curve of  $\mu = 1 + 2\kappa + 3\kappa^2$ .

We would generally expect the shear,  $\gamma$ , to fluctuate strongly for light rays passing through regions of high density (high convergence), and we indeed find considerable scatter in the shear when plotted against the convergence. Figure 10, however, shows the result of binning the convergence values and calculating the average shear in each bin, for sources at  $z_s = 4$ . We see that throughout most of the range in  $\kappa$  the average shear increases very slowly, and closely linearly. (At the high  $\kappa$  end there are too few data points to establish accurate average values for  $\gamma$ .) This result suggests that there may be a contribution to the mag-

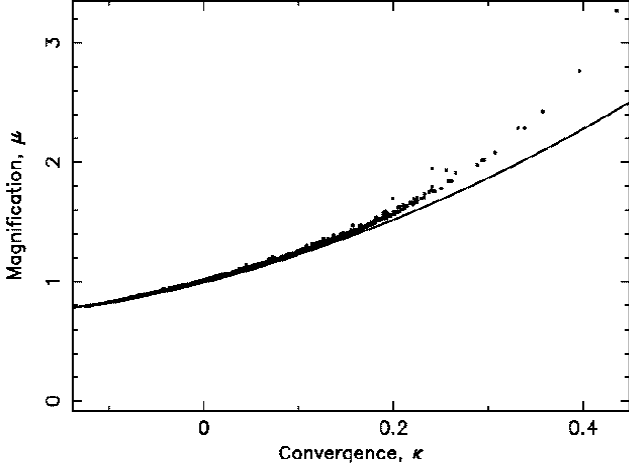


**Figure 9.**  $\mu$  vs.  $\kappa$  for  $z_s = 4$  (dots). The continuous line, shown for comparison, represents  $\mu = 1 + 2\kappa + 3\kappa^2$ .

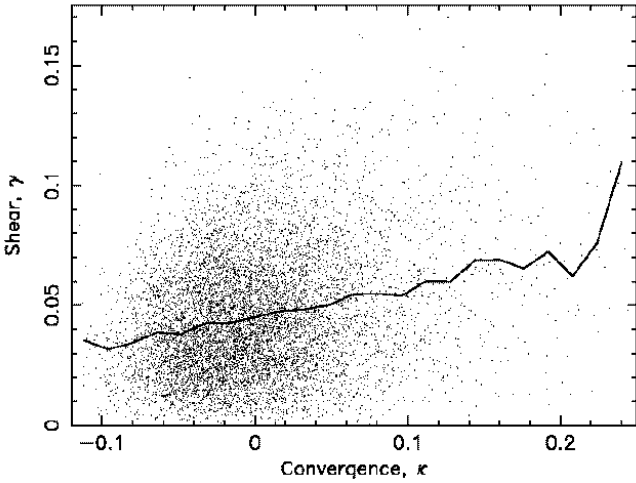
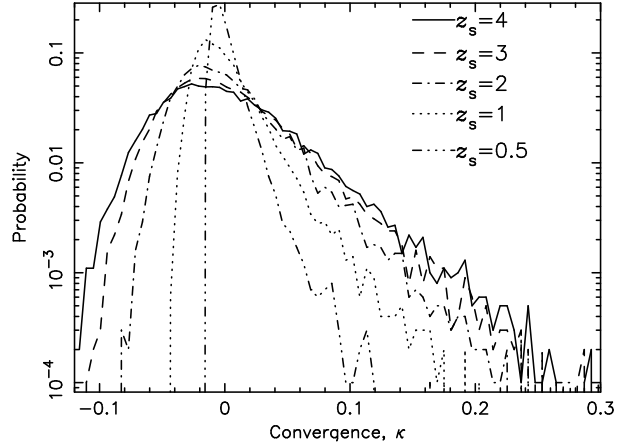


**Figure 10.** Shear vs. convergence for sources at  $z_s = 4$  (dots), and the average shear (full line) in each of the  $\kappa$  bins, which shows a slow and nearly linear increase with increasing convergence.

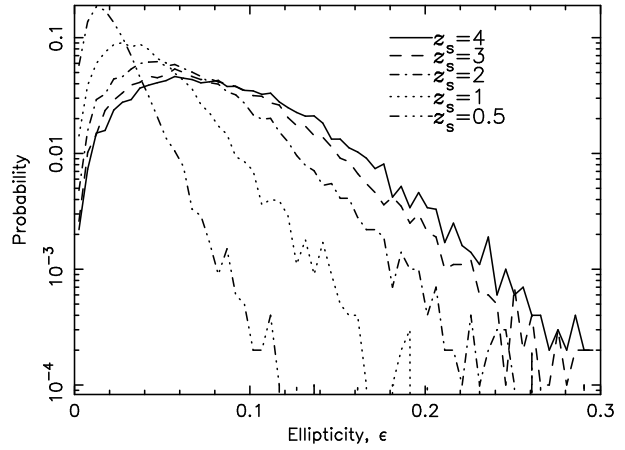
nification from the shear, and we discuss this later in this Section.

Figure 11 shows the distributions in the convergence,  $\kappa$ , primarily responsible for the magnifications. The rms values for the convergence are 0.052 (for  $z_s = 4$ ), 0.047 (for  $z_s = 3$ ), 0.038 (for  $z_s = 2$ ), 0.025 (for  $z_s = 1$ ) and 0.013 (for  $z_s = 0.5$ ). These values are entirely consistent with the rms fluctuations for the magnification about the mean (stated above), being slightly below half the rms magnification values (see equation 14).

The distributions in the shear,  $\gamma$ , (defined according to equation 12) for the five source redshifts, are broadest, as expected, for the highest source redshifts, and, for  $z_s = 4$ , 97½% of all lines of sight have shear values below 0.103. The ellipticity,  $\epsilon$ , in the image of a source is primarily produced by the shear, and we show in Figure 12 the distributions in  $\epsilon$  for the five source redshifts. The peaks in the ellipticity



**Figure 11.** The probability distributions for the convergence,  $\kappa$ , for the five different source redshifts.



**Figure 12.** The probability distributions for the ellipticity,  $\epsilon$ , for the five different source redshifts.

distributions occur at  $\epsilon = 0.057$  for  $z_s = 4$ , 0.057 for  $z_s = 3$ , 0.047 for  $z_s = 2$ , 0.027 for  $z_s = 1$  and 0.012 for  $z_s = 0.5$ . Figure 13 displays the accumulating number of lines of sight with  $\epsilon$  greater than the abscissa value. For  $z_s = 4$ , we find that 97½% of all lines of sight have ellipticities up to 0.195. In Figure 14 we see that the ellipticity is very closely linear in terms of  $\gamma$  throughout most of the range in  $\gamma$ . The scatter arises because of the factor containing the convergence,  $\kappa$ , in equation 16.

Finally, we attempted to see if there was a contribution to the magnification from the shear as implied by the distance-redshift relation (equation 3). We found considerable scatter, as expected, in the plots of magnification vs. shear, but we found in Figure 10 a tenuous connection between the shear and the convergence, indicating that there may be a similar connection between the magnification and the shear. We see from equation 14 that the effect of shear is only of second order (as established by Schneider and Weiss, 1988a). By binning the shear values and calculating the av-

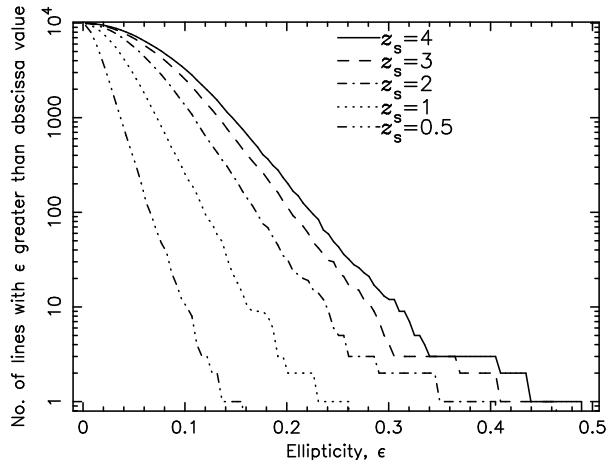


**Figure 13.** The accumulating number of lines of sight with  $\epsilon$  greater than the abscissa value, for the five source redshifts.

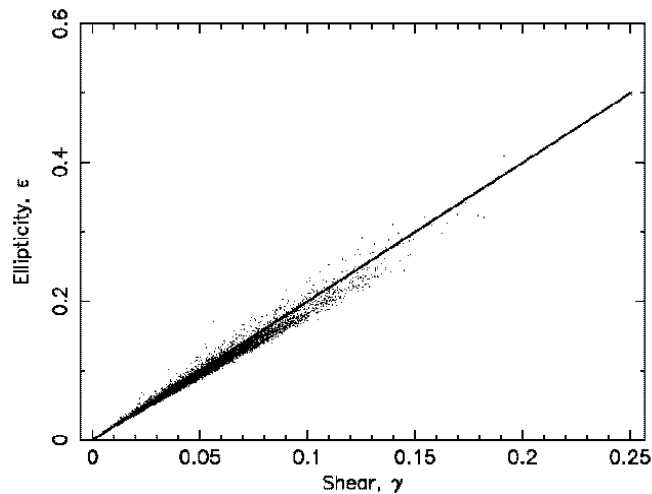


**Figure 14.** Source ellipticity vs. shear for  $z_s = 4$  (dots). The straight line, shown for comparison, represents  $\epsilon = 2\gamma$ .

erage magnification in each bin, we are able to show (Figure 15) that there may be a slow increase in  $\langle \mu \rangle$  with increasing shear. Figure 15 is for sources at  $z_s = 4$ . Although there are insufficient data points at the high shear end, it still seems likely that the effects of shear on the mean magnification may be at least 10% for shear values greater than about 0.1. However, interestingly, only 2.6% of the data points in our simulation produced shear in excess of 0.1. According to equation 3, the shear has an effect in the distance-redshift relation equivalent to increasing the effective smoothness parameter,  $\bar{\alpha}$ . However, by substituting the mean shear value determined for sources at  $z_s = 0.5$  the effect on  $\bar{\alpha}$  is found to be completely negligible. Furthermore, the importance of the effect reduces with redshift, so that our conclusion in Section 3, to ignore the effects of shear in the distance-redshift relation, can now be justified.

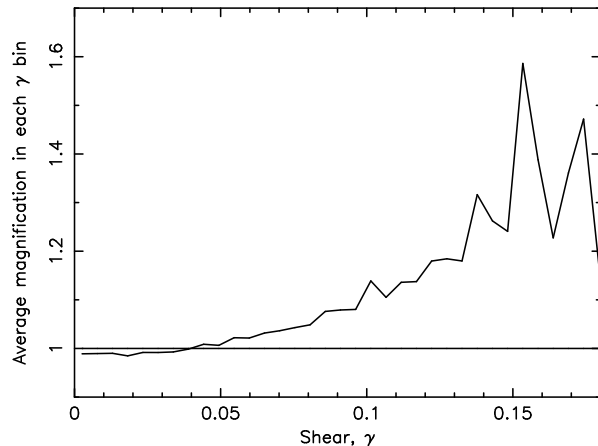


**Figure 15.** The average magnification in each shear bin, for sources at  $z_s = 4$ . The overall mean magnification at  $\langle \mu \rangle = 1$  is shown for comparison.

## 7 DISCUSSION OF RESULTS

Following the brief summary in the Introduction of work by other authors on the effects of weak gravitational lensing in the  $s$ CDM cosmology, we described in Section 2 the algorithm for the three-dimensional shear, and some of the key advantages it offers over other methods. In particular, we mentioned the ability of the code to include automatically the effects of matter in the periodic images of the fundamental volume, so that matter effectively stretching to infinity is included in computations of the shear. We also described the variable softening feature in the code which allows a good physical interpretation of the matter distribution in simulation time-slices to be made. We explained our choice of an appropriate minimum for the variable softening, taking into account its physical dimension, the degree of particle clustering, and the likelihood of strong lensing effects. We also described in Section 2 the  $s$ CDM simulations we have used, which are available from the Hydra consortium.

One clear advantage of the algorithm operating on a three-dimensional volume is that we can apply the appropriate angular diameter distance to every single evaluation position, thereby avoiding the introduction of errors associated with the use of single values in two-dimensional methods. (Couchman et al., 1998, analyses these possible errors.) However, we have had to consider what the ‘appropriate’ values should be.

First, we considered the effects of shear in the distance-redshift relation (equation 3), and were guided by the findings of Schneider and Weiss (1988a), Watanabe and Tomita (1990) and Futamase and Sasaki (1989) that the shear probably has only a second order effect. Our decision to ignore the effects of shear in the relation in general is justified because we found that significant effects may occur only in  $\sim 2.6\%$  of the lines of sight, and the impact on the effective value of the smoothness parameter,  $\bar{\alpha}$ , by substituting the mean values of the shear, is completely negligible at all redshifts.

Second, we needed to include a suitable value for the smoothness parameter,  $\bar{\alpha}$ . The minimum value for the vari-

able softening in the shear algorithm, and the number of particles falling within this minimum value, provides an excellent framework for determining  $\bar{\alpha}$  in accordance with the original definition of Dyer and Roeder (1972).

We find, on this definition, that  $\bar{\alpha}$  varies between approximately 1.0, in the  $z = 3.6$  time-slice, and 0.9, at  $z = 0$ , and we therefore checked the significance for the angular diameter distance multiplying factor with these extreme values. For sources at  $z_s = 4$  the difference between the factors is very small (see Figure 2) at all lens redshifts, and the maximum discrepancy is only 3.1%, as shown in Figure 3. This discrepancy is always less than 1% for sources with redshifts less than 1. Furthermore, we investigated the effects of  $\bar{\alpha}$  on the magnification distribution arising from a single (assumed isolated) simulation box at  $z = 0.5$  for a source at  $z_s = 4$ . The two distributions are virtually indistinguishable; the most significant difference is in the values of the maximum magnification in each case, which differs by only 1.9%. For these reasons we chose to proceed with our analysis of the results for the sCDM cosmology on the basis of  $\bar{\alpha} = 1$ .

In Section 4 we found the general and interesting result that the rms values of the ‘intrinsic’ computed shear values, multiplied by the conversion factor  $B(1+z)^2$ , but before the application of the angular diameter distance multiplying factors, fell slowly with redshift towards  $z = 0$ , (i.e., with the evolving and expanding universe). Evidently, the universal expansion just outweighs the formation of structure when viewed in terms of the shearing on light. The formation of structure could be seen by considering only the sets of highest values in each time-slice, and then the mean values of these initially fall, before increasing slowly at the onset of structure formation. When the appropriate angular diameter distance multiplying factors were applied to the computed values, we then found the further interesting result that there can be considerable contributions to the shear and magnification arising from time-slices covering a very broad range of redshifts. This result is displayed in Figure 5.

In Section 5 we described how the data computed from our sets of simulation boxes were manipulated in accordance with the multiple lens-plane theory to produce the results of Section 6. There we showed results based on sources at five different redshifts, namely  $z_s = 4, 3, 2, 1$  and 0.5. We showed distributions in the magnification (and details of the high magnification end of these distributions), the convergence and the ellipticity (which closely resembles the distribution in the shear), and also the relationships amongst these various quantities. Figure 9 shows the strong departure from the linear regime for the magnification as a function of the convergence, whilst Figure 14 shows a closely linear relationship between the ellipticity and the shear. Figure 10 suggests a slow increase in shear with increasing convergence, broadly as expected. For sources at  $z_s = 4$ , 97½% of all lines of sight have magnification values up to 1.30. (The maximum magnifications depend on the choice of the minimum softening in the code, although the overall distributions are very insensitive to the softening.) In particular, we found rms fluctuations in the magnification (about the mean) as much as 0.13 for sources at  $z_s = 4$ . Even for sources at  $z_s = 0.5$  there is a measurable range of magnifications up to 1.05 for 97½% of the lines of sight.

We summarised in the Introduction the methods of other workers using the sCDM cosmology. Because of the way in which Jaroszyński et al. (1990) determine the magnifications, their distributions do not have mean magnifications of 1. However, their dispersions in the convergence for sources at  $z_s = 1$  and  $z_s = 3$  can be seen to be considerably lower than our values. In addition the dispersions appear to show very little evolution with redshift. Wambsganss et al. (1998) find magnifications up to 100 and correspondingly highly dispersed distributions, very much larger than ours at  $z_s = 3$ . (Their magnification distributions show separately the results for multiply-imaged sources and singly-imaged sources.) The very wide distributions they find have also enabled them to support a  $\mu^{-2}$  power-law tail in the distribution which is predicted by Schneider et al. (1992) in the case of magnification by point sources when  $\mu \gg 1$ . The magnification distributions of Premadi et al. (1998a) appear incomplete, but the range in magnifications appears to be rather similar to ours for sources at  $z_s = 3$ . This is reassuring because, although their method relies on two-dimensional projections of the simulation boxes, they include many of the essential features to which we have drawn attention, for example, an assumed periodicity in the matter distribution, randomly chosen initial conditions to avoid structure correlations between adjacent simulation boxes, the net zero mean density requirement, realistic mass profiles for the particles, and use of the filled beam approximation with a smoothness parameter,  $\bar{\alpha} = 1$ . Marri and Ferrara (1998) show very much wider magnification distributions than we have found, and also very high maximum values, which occur as a result of using point particles rather than smoothed particles. We also disagree with their choice of  $\bar{\alpha} = 0$ , which is representative of an entirely clumpy universe, as opposed to our finding that the sCDM universe is very close to being smooth (with  $\bar{\alpha} \simeq 1$ ) at all epochs.

In our own work 97½% of the lines of sight have ellipticities up to 0.195 for  $z_s = 4$ . At the peaks of the distributions we found values of 0.057 and 0.027 for  $\epsilon$  for sources at  $z_s = 3$  and 1 respectively. These are somewhat lower than the values of 0.095 ( $z_s = 3$ ) and 0.045 ( $z_s = 1$ ) found by Jaroszyński et al. (1990). Rather surprisingly, however, their peak values in the distributions for the shear are quite similar to our own, especially for sources at  $z_s = 3$ .

Our magnification results may have an impact on the interpretation of the magnitude data for high-redshift Type Ia Supernovæ reported by Riess, Filippenko, Challis et al. (1998), since we have seen in Section 6 the possible range of magnifications that may apply to distant sources. The high-redshift Supernovæ data include sources up to redshifts of 0.97, so that the effects of the large-scale structure should not be ignored when interpreting the peak magnitudes and distance moduli. However, our magnification values for  $z_s = 1$  and  $z_s = 0.5$  above and below which 97½% of all lines of sight fall are considerably closer to unity than the values found by Wambsganss, Cen, Xu and Ostriker (1997) for the sCDM model. We would therefore expect to find correspondingly smaller lensing-induced dispersions in the distance moduli. However, we hope to quantify the dispersions in the distance moduli and the effect on the deceleration parameter,  $q_0$ , for an open cosmology in a future paper, especially in view of Riess et al.’s (1998) conclusions in favour of an open universe with a cosmological constant.

Another area affected by the presence of a distribution in magnifications is the luminosity function for quasars or high-redshift galaxies. Most sources are demagnified (the median value for  $\mu$  is always just less than 1) which will remove many galaxies from the dim end of the luminosity function in a flux-limited survey, but at  $z_s = 2$ , say, we find an rms fluctuation in the magnifications of 8.8% which will also allow some dim galaxies to be magnified and observed, where otherwise they would not have been.

In addition to considering these matters further we hope to address the following questions in the immediate future.

1. How does the redshift dependence of the shear matrix change in low-density universes? We shall be attempting to answer this question using simulation data from other cosmologies available from the Hydra consortium. In particular, we shall work on open and flat cosmological simulations with  $\Omega_0 = 0.3$ . Of particular interest is the flat model with  $\Omega_0 = 0.3$  and cosmological constant  $\Lambda_0 = 0.7$ , in view of the recent work by Riess et al. (1998) indicating the likelihood of this type of universe. In critical density universes it is believed that clustering continues to grow to the present day, and this is indicated by the results shown in Figure 4. However, in low density universes, structures should have formed by  $z \sim \Omega_0^{-1} - 1$ , so that the shapes of the curves in Figure 4 are likely to be very different.

2. How do our distributions in the magnification, ellipticity, shear and convergence vary amongst different cosmologies? With low-density universes, weak lensing effects are likely to be very different due to four main factors: (i) the formation of structure at earlier times, and its persistence through periods in which the contribution to the lensing is significant; (ii) dilution of the effects as the universe expands beyond the formation of structure; (iii) different values for the angular diameter distances; (iv) the lower average values for the computed shear components in view of the lower density values in the universe.

3. Do the high-magnification and low-ellipticity lines of sight occur because of the effects of individual large clusters, or as a result of continuous high density regions such as filamentary structures?

4. How frequently do lines of sight in the direction of multiply-imaged quasars coincide with lines of high convergence associated with the general form of the large-scale structure (independent of the lensing galaxy)? There is clear evidence (Thomas, Webster & Drinkwater, 1995) of increased numbers of near-neighbour galaxies (when viewed along the line of sight) to bright quasars, and this raises the intriguing possibility that some sub-critical lenses may become critical (and produce multiple images of background sources) in the presence of high density large-scale structure along the line of sight. According to the multiple lens-plane theory it is entirely consistent that the determinant of the developing Jacobian matrix along a high-convergence line of sight may change sign in the presence of a high surface density (but sub-critical) lens. In such a scenario modifications to the models for the surface density profile of the lensing galaxy would also be required.

## ACKNOWLEDGMENTS

We are indebted to the Starlink minor node at the University of Sussex for the preparation of this paper, and to the University of Sussex for the sponsorship of AJB. We thank NATO for the award of a Collaborative Research Grant (CRG 970081) which has greatly facilitated our interaction. R. L. Webster and C. J. Fluke of the University of Melbourne, and K. Subramanian of the National Centre for Radio Astrophysics, Pune, have been particularly helpful.

## REFERENCES

- Blandford R. D. & Narayan R., 1986, *Ap. J.*, 310, 568  
 Blandford R. D. & Kochanek C. S., 1987, *Proc. 4th Jerusalem Winter School for Th. Physics, Dark Matter in the Universe*, ed. Bahcall J. N., Piran T. & Weinberg S., Singapore, World Scientific, p.133  
 Couchman H. M. P., Barber A. J. & Thomas P. A., 1998, *astro-ph*, 9810063, Preprint  
 Couchman H. M. P., Thomas, P. A., & Pearce F. R., 1995, *Ap. J.*, 452, 797  
 Dyer C. C. & Roeder R. C., 1972, *Ap. J. (Letts.)*, 174, L115  
 Dyer C. C. & Roeder R. C., 1973, *Ap. J. (Letts.)*, 180, L31  
 Falco E. E., Govenstein M. V. & Shapiro I. I., 1991, *Ap. J.*, 372, 364  
 Fluke C. J., Webster R. L. & Mortlock D. J., 1998a, *astro-ph*, 9812300, Preprint  
 Fluke C. J., Webster R. L., Mortlock D. J., 1998b, In preparation  
 Futumase T. & Sasaki M., 1989, *Phys. Rev. D*, 40, 2502  
 Grogan N. A. & Narayan R., 1996, *Ap. J.*, 464, 92  
 Hockney R. W. & Eastwood J. W., 1988, 'Computer Simulation Using Particles', IOP Publishing, ISBN 0-85274-392-0  
 Jaroszyński M., 1991, *MNRAS*, 249, 430  
 Jaroszyński M., 1992, *MNRAS*, 255, 655  
 Jaroszyński M., Park C., Paczynski B., & Gott III J. R., 1990, *Ap. J.*, 365, 22  
 Keeton C. R. & Kochanek C. S., 1997, *Ap. J.*, 487, 42  
 Kovner I., 1987, *Ap. J.*, 316, 52  
 Marri S. & Ferrara A., 1998, *astro-ph*, 9806053, Preprint  
 Peacock J. A. & Dodds S. J., 1994, *MNRAS*, 267, 1020  
 Premadi P., Martel H. & Matzner R., 1998a, *Ap. J.*, 493, 10  
 Premadi P., Martel H. & Matzner R., 1998b, *astro-ph*, 9807127, Preprint  
 Premadi P., Martel H. & Matzner R., 1998c, *astro-ph*, 9807129, Preprint  
 Riess A. G., Filippenko A. V., Challis P., Clocchiatti A., Diercks A., Garnavich P. M., Gilliland R. L., Hogan C. J., Jha S., Kirshner R. P., Leibundgut B., Phillips M. M., Reiss D., Schmidt B. P., Schommer R. A., Smith R. C., Spyromilio J., Stubbs C., Suntzeff N. B. & Tonry J., 1998, *A. J.*, 116, 1009  
 Schneider P., Ehlers J., & Falco E. E., 1992, 'Gravitational Lenses', Springer-Verlag, ISBN 0-387-97070-3  
 Schneider P. & Weiss A., 1988a, *Ap. J.*, 327, 526  
 Schneider P. & Weiss A., 1988b, *Ap. J.*, 330, 1  
 Thomas P. A., Webster R. L. & Drinkwater M. J., 1995, *MNRAS*, 273, 1069

- Tomita K., 1998, astro-ph, 9806047, Preprint  
Vianna P. T. P., & Liddle A. R., 1996, MNRAS, 281, 323  
Wambsganss J., Cen R., & Ostriker J., 1998, Ap. J., 494, 29  
Wambsganss J., Cen R., Xu G. & Ostriker J., 1997, Ap. J.,  
475, L81  
Watanabe K. & Tomita K., 1990, Ap. J., 355, 1